Technical Report Documentation Page

1. Report No.	2. Government Accession No.	3. Recipient's Catalog No.

4. Title and Subtitle	5. Report Date
	6. Performing Organization Code

7. Author(s)	8. Performing Organization Report No.

9. Performing Organization Name and Address	10. Work Unit No. (TRAIS)
	11. Contract or Grant No.

12. Sponsoring Agency Name and Address	13. Type of Report and Period Covered
	14. Sponsoring Agency Code

15. Supplementary Notes

16. Abstract

17. Key Words	18. Distribution Statement

19. Security Classif. (of this report)	20. Security Classif. (of this page)	21. No. of Pages	22. Price
Unclassified	Unclassified		

Form DOT F 1700.7 (8-72)   Reproduction of completed page authorized

Impact of Design Constraints on Noise and Emissions of Derivative Supersonic Engines

Prakash Prashanth,[*] Laurens J. A. Voet,[†] Raymond L. Speth,[‡] Jayant S. Sabnis,[§] Choon S. Tan,[¶] and Steven R. H. Barrett[**]

Massachusetts Institute of Technology, Cambridge, Massachusetts 02139

https://doi.org/10.2514/1.B38918

The propulsion systems used in commercial supersonic transport (SST) aircraft, such as the Concorde, have used repurposed engines or derivative engines based on cores from existing donor engines rather than purpose-designed clean-sheet engines. A similar approach is currently being adopted in the development of new SSTs. Turbomachinery components and cooling mass flow rates in derivative engines are sized by the design cycle of the donor engine and constrain the design of the derivative engine cycle. Here, we identify the constraints imposed by the donor engines and quantify their impact on the specific fuel consumption (SFC), certification noise, and NO$_x$ (oxides of nitrogen) emissions index [EI(NO$_x$)] relative to purpose-designed clean-sheet engines. We design and optimize a clean-sheet and derivative engine for a notional 55 metric ton SST proposed by NASA. A clean-sheet engine optimized for SFC results in an approximately 4.5% reduction in SFC, an approximately 2.5-fold increase in EI(NO$_x$), and a 1.2 EPNdB increase in certification noise relative to the derivative engine. Applying a constraint on EI(NO$_x$) to the clean-sheet engine results in an approximately 0.5% reduction in SFC relative to the derivative engine. The work provides a quantitative comparison of clean-sheet purpose-built engines and derivative engines from an environmental perspective that can inform policy makers as they develop updated environmental standards for civil supersonic aircraft.

Nomenclature

a_0	=	ambient speed of sound, m/s
D	=	fan diameter, m
D_p	=	certification mass of emissions
c_p	=	specific heat capacity, J/kg/K
EI	=	emission index, g/kg
EPNL	=	effective perceived noise level, Effective Perceived Noise (EPNdB)
ER	=	extraction ratio ($P_{t1.6}/P_{t6}$)
FAR	=	fuel/air ratio
F_{oo}	=	rated thrust for certification
f_{corr}	=	($\dot{m}_f \mathrm{LHV}/a_0 D^2 p_0$); corrected fuel flow rate
L/D	=	lift to drag ratio
LHV	=	lower heating value, J/kg
$\dot{m}_f$	=	mass flow rate of fuel, kg/s
$\dot{m}_i$	=	mass flow rate at station i, kg/s
N	=	spool speed, rpm
$P_{t,i}$	=	total pressure at station i, Pa
SFC	=	specific fuel consumption, kg/s/kN
$T_{t,i}$	=	total temperature at station i, K
V_{jet}	=	jet velocity, m/s
δ_i	=	P_i/P_{STD}, where $P_{STD} = 101.325$ kPa
θ_i	=	T_i/T_{STD}, where $T_{STD} = 298.15$ K
π_{oo}	=	overall pressure ratio at rated thrust

I. Introduction

THERE has been recent growth in interest in the development of civil supersonic transport (SST), with several new aircraft designs being pursued by the industry [1,2]. However, although emissions standards for subsonic aircraft have been updated four times since they were first adopted in 1981 [3], the existing environmental regulations for supersonic aircraft are based on the Concorde, and their relevance today is unclear. Literature suggests that the environmental impact of SST is different from subsonic aircraft and will be one of the major challenges for their public acceptance and commercial success [4–6]. The International Civil Aviation Organization (ICAO) is considering new environmental standards for future commercial supersonic aircraft because gas turbine engines for supersonic applications have significantly different operating conditions than their subsonic counterparts. Engines designed for SST aircraft need to operate at both subsonic and supersonic conditions during different phases of flight and typically operate at higher altitudes (12–18 km) than subsonic aircraft (10–12 km). Furthermore, the aerodynamics of supersonic flight, such as the presence of wave drag, result in a stronger coupling between the airframe and the propulsion system than in a subsonic aircraft. This coupling imposes additional size constraints on the engine inlet to minimize overall aircraft drag, which typically implies a constraint on the maximum fan diameter that can be used. Additionally, the low-speed aerodynamic characteristics of these airplanes require relatively high-speed takeoff and landing, compared to subsonic aircraft, corresponding to higher operating takeoff and landing thrust [7]. These differences in flight conditions and propulsion system requirements impact performance metrics such as fuel consumption, pollutant emissions, and noise during takeoff and landing.

The development of propulsion systems for supersonic applications can range from purpose-built, clean-sheet designs to the adoption of existing production engines. Historically, propulsion systems for civil supersonic transport were adapted from existing engines to meet the propulsion requirements of the new application. The Rolls–Royce Olympus 593 engine that powered the last civil supersonic aircraft, Concorde, was derived from an engine developed for a military aircraft: the Avro Vulcan [8]. Similarly, companies that are currently developing civil supersonic aircraft have proposed propulsion system concepts based on the cores of existing gas turbine engines used for subsonic application, without the use of an afterburner. Proposed propulsion

systems such as the General Electric Affinity engine [9] combine the core (consisting of the high-pressure compressor, combustor, and high-pressure turbine) of a subsonic donor engine with a new low-pressure spool (fan and low-pressure turbine) and necessary modifications to the inlet (supersonic diffuser) and exhaust (variable nozzle area). While the engine can be adapted in other forms, such as scaling existing cores and the modification of certain compressor or turbine stages, for this work, we define a derivative engine as using an existing core from a donor engine without any modifications, along with a new low-pressure spool.

The differences in operating conditions and requirements of the propulsion systems between subsonic donor engines and supersonic derivative engines suggests that the performance of these derivative engines might be suboptimal relative to purpose-built engines for the same supersonic application. However, the fuel burn, emissions, and noise of a derivative engine relative to a clean-sheet engine have not previously been quantified. Quantifying the environmental performance of derivative engines relative to clean-sheet engine designs will help inform policy makers and other stakeholders while developing new environmental standards. In this work, we identify how the constraints imposed by the donor core affect the feasible design space for the derivative engine for the SST using a first-principles approach. This work provides the first estimate of the noise and emissions of a derivative engine as a function of the constraints imposed by the donor core and demonstrates these impacts on the NASA Supersonic Technology Concept Airplane (STCA).

II. Methods

The constraints imposed by the donor engine core on the design space of the derivative engine are analyzed by comparing the relative performance of the derivative engine against a clean-sheet design. The differences in fuel burn, engine certification noise, and NO_x emissions are quantified using an engine cycle model, the P_3-T_3 method to calculate NO_x emissions, and the certification noise levels are calculated using standard noise source models [10] on the NASA STCA Standard takeoff and approach trajectory following the work of Berton et al. [11]. The following sections detail the methods used to model the engine thermodynamic cycle, calculate the NO_x emissions index (EI), and the certification noise level.

Table 1 Propulsion system requirements (per engine) for the STCA; the top-of-climb conditions are chosen as the aerodynamic design point for any component that is purpose designed for the application

	SLS	Takeoff	Top of climb	End of cruise
Altitude, km	0	0	12.5	15.5
Altitude, ft	0	0	41,000	51,000
Mach	0	0.25	1.4	1.4
Net thrust, kN	74	63	24	15
Net thrust, lbf	16,620	14,140	5,500	3,300

A. Mission Analysis and Propulsion System Requirements

The STCA designed by NASA is a 55 tonne aircraft with a design range of 4240 nmi (7852 km), carrying eight passengers and cruising at Mach 1.4 at altitudes between 44,000 and 51,000 ft (13.4 and 15.5 km), powered by three derivative engines based on the CFM56-5B3 engine [11]. The aerodynamic characteristics of the STCA airframe are used in this work to define the propulsion system requirements and the subsequent impact of design space constraints on the performance, emissions, and noise of derivative engines relative to purpose-built clean-sheet engines for supersonic application.

The derivative and clean-sheet engine are designed to meet the propulsion system requirements of the NASA STCA, as summarized in Table 1. The top-of-climb and end-of-cruise thrust requirements correspond to a rate of climb of 810 ft/min (4.1 m/s) (at a weight of 111,000 lb or 494 kN and L/D of 7.35) and 200 ft/min (1 m/s) (at a weight of 61,500 lb or 274 kN and L/D of 6.5). An engine is modeled to meet the requirements at multiple mission points as shown in Table 1. The top-of-climb conditions are chosen as the aerodynamic design point (ADP) for any component that is being designed. This does not apply to the donor core because the ADP for the donor core is determined by the donor engine cycle.

B. Propulsion System Design

The CFM56-5B3 engine is chosen as the donor engine for the derivative engine core, consistent with the work of Berton et al. [11] in which the STCA aircraft was designed with a CFM56-5B3 based derivative engine. A model drawing of the donor engine architecture is shown in the bottom half of Fig. 1. The low-pressure spool of the donor engine consists of a fan and low-pressure compressor (LPC), powered by the low-pressure turbine (LPT); the high-pressure spool consists of a high-pressure compressor (HPC) powered by the high-pressure turbine (HPT) that, along with the combustor, constitute the core of the engine. The top half of Fig. 1 shows the derivative engine which uses the same core components HPC, combustor, and HPT (shown in red, labeled as common core in Fig. 1] as the donor engine (shown on the bottom half). This core taken from the donor engine is assumed to be used in the derivative engine without any modifications. The derivative engine has a purpose-designed low-pressure spool as well as a supersonic inlet and a mixed-flow nozzle.

The Numerical Propulsion System Simulation (NPSS) software [12] is used to develop a thermodynamic cycle model of the donor engine. The thrust produced by the donor engine as a function of fuel flow rate, as calculated by the NPSS model, is validated against publicly available certification data maintained by European Aviation Safety Agency (EASA) in the ICAO Aircraft Engine Emissions Databank (EDB) [13], as shown in Fig. 2. The allowable measurement uncertainty in the fuel flow data presented in the EDB is ±2%, while the uncertainty in the engine thrust is ±1% at rated thrust and ±5% at the lowest thrust setting [3]. The root mean squared (RMS) error between the fuel flow calculated from the NPSS model and the EDB data is 1.3% across all the thrust values. The component
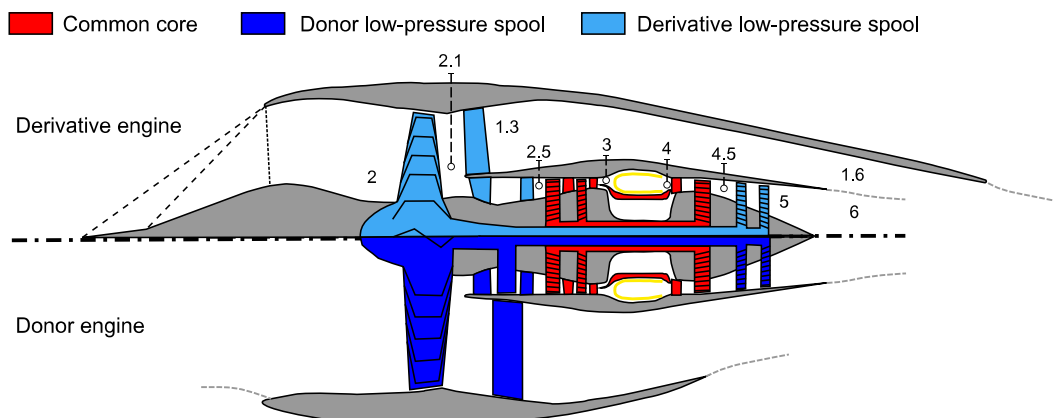

Fig. 1 Engine architecture schematic. The lower half shows the subsonic donor engine. The high-pressure spool (red) is used in the derivative engine (top half) along with modifications to the inlet, fan, and nozzle as shown on the top half of the figure.
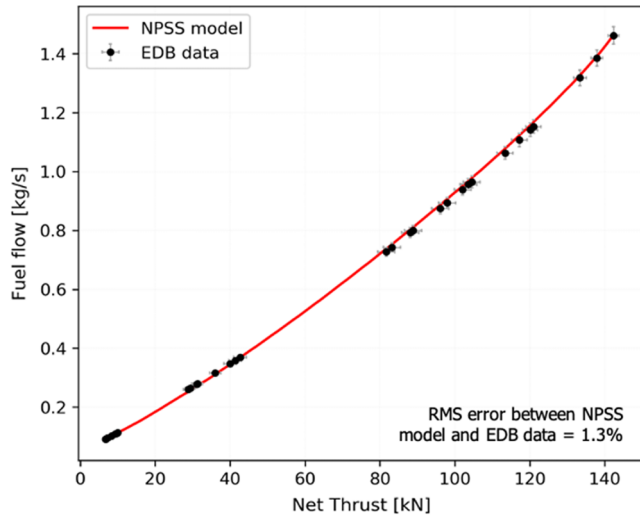
Fig. 2 Comparison of CFM56-5B3 thrust vs fuel flow characteristic for NPSS engine model and engine EDB. The uncertainty bars show the allowed measurement uncertainty in the fuel flow and thrust measurements as reported in the EDB.

characteristics such as efficiency and pressure ratio of the turbomachinery were thus calibrated. A summary of the CFM56-5B3 NPSS donor engine model characteristics at sea-level static (SLS) conditions is given in Appendix A.

As shown in the engine architecture diagram in Fig. 1, the derivative engine uses the high-pressure core of the donor engine. The low-pressure spool consists of a fan and a LPT. An external compression supersonic inlet with two oblique shocks is mounted upstream of the fan, with the pressure recovery modeled using standard oblique shock equations [14]. A fully mixed, variable area nozzle is added downstream of the LPT. The engine is designed such that the nozzle pressure ratio is approximately 2.0 at takeoff conditions, which keeps the flow just choked to avoid shock-cell noise. Polytropic efficiencies (obtained via calibration of the NPSS donor engine model as described previously) of the turbomachinery components at their design points are fixed to the CFM56-5B3 technology level. The dimensional quantities characterizing the engine cycle, such as the flow areas and the cooling bleed flow fractions of the donor engine core, are treated as fixed constants in the derivative engine model, thereby representing the use of the donor core without any modifications. This means that, during the design of the derivative engine, the HPC, HPT, and combustor are not sized but are instead operated at off-design conditions, while the fan and LPT are sized (i.e., the map scalars of the high-pressure turbomachinery, the flow areas, and the cooling bleed flow fractions of the CFM56-5B3 donor engine core are held constant).

The engine architecture for the clean-sheet design is the same as for the derivative design. However, all the components for the clean-sheet engine along with the high-pressure core are purpose designed. The maximum polytropic efficiencies of the turbomachinery components in the clean-sheet design are set to the CFM56-5B3 values to model the same technology level. The turbine cooling flow requirements are sized according to the semi-empirical method from Gauntner [15].

C. Sensitivity of Clean-Sheet and Derivative Engines to Propulsion System Requirements

An optimizer coupled with the NPSS models described here is used to optimize the engine cycle subject to constraints such as the turbine metal temperature and fan diameter. To quantify the sensitivity of the optimal clean-sheet and derivative engines to the propulsion system requirements, the optimization is repeated for a sweep of parameters of interest. Specifically, the impact of a change in engine thrust requirement (corresponding to an airframe weight increase for a fixed L/D characteristic) is assessed for a fixed set of flight conditions (cruise Mach number and altitude). A $\pm 5\%$ variation in thrust required relative to the STCA aircraft [11] is considered

because this might be representative of typical thrust requirement growth during an aircraft development program.

D. Quantifying Engine NO$_x$ Emissions

The formation of NO$_x$ in nonpremixed gas turbine combustors (especially at cruise and takeoff) is dominated by thermal NO production via the Zeldovich mechanism [16]. The production rate of NO is a function of the flame temperature and the residence time. In a rich font-end combustor, the stoichiometric flame temperature is a function of the inlet temperature of the gas, and therefore the combustor inlet temperature T_{t3} can be used to estimate the production of NO$_x$, and then a pressure correction can be performed to account for the reduced ambient pressure at cruise using the combustor inlet pressure P_{t3}. This method is known as the P_3-T_3 method [17]. In an engine designed for supersonic cruise, the freestream flow is decelerated by a series of shocks in the intake to approximately Mach 0.5–0.6 at the fan face to be compatible with the fan. The operating Mach number of downstream components after the intake is no different from an engine designed for subsonic aircraft. The only impact of the increased cruise Mach number of supersonic aircraft manifests as an increase in total temperature and pressure at the inlet to the first compressor (or fan) blade due to the ram compression. A comparison between the P_3-T_3 method based estimate of the EI(NO$_x$) of the Olympus 593 engine to in-flight measurement of EI(NO$_x$) in the plume of the Concorde was conducted by Fahey et al. [18], and the empirical estimates were found to be within 20% of the measurements. The cruise Mach number of the Concorde during these in-flight measurements was Mach 1.97 at an altitude of 16.1 km, further supporting the applicability of the P_3-T_3 for engines designed for supersonic cruise.

The P_3-T_3 method [17] is therefore used to estimate the emission index of NO$_x$ for a given engine operating condition in this work. The emission index of NO$_x$ is assumed to be proportional to $P_{t3}^{0.4}$ [17], and a polynomial fit in T_{t3} is constructed based on sea-level EDB emission index data for the CFM56-5B3 based on standard-day absolute humidity,

$$\frac{EI(\text{NO}_x)}{P_{t3}^{0.4}} = 6.26 \cdot 10^{-8} T_{t3}^3 - 0.001171 \cdot T_{t3}^2 + 0.0737 \cdot T_{t3} - 15.04$$

(1)

where temperature is in kelvin, pressure is in kilopascals, and EI(NO$_x$) is in grams of NO$_x$ per kilogram of fuel. This polynomial fit and the corresponding EDB data are shown in Fig. 3. The root mean squared error of the P_3-T_3 model relative to the certification data is 0.33 g/kg. Because the emissions for rich front-end combustors are largely controlled by the flame temperature and quenching of the primary zone effluents, it is assumed that the regression model for NO$_x$ based on the donor CFM56-5B3 engine is representative of the emissions trends for the same combustor used in the derivative and
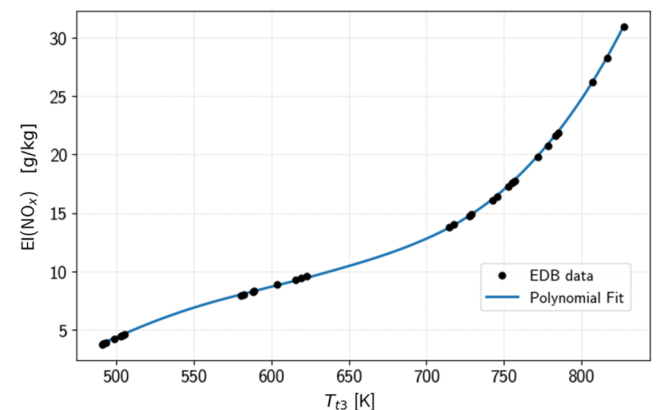

Fig. 3 EDB emission indices data of the CFM56-5B3 approximated by a polynomial fit following the P_3-T_3 method [see Eq. (1)].

clean-sheet engines. Emissions of NO_x at cruise are calculated by applying humidity corrections to Eq. (1) at altitude [17].

E.   Quantifying Engine Noise

The aircraft certification cumulative noise levels are computed using the open-source aircraft noise estimation model, pyNA [19], that is an implementation of the methods outlined by Zorumski [10]. The noise sources modeled in pyNA account for the fan broadband and tones, the core noise, the jet mixing noise, and the airframe noise. Further details on the modeling of the noise sources and propagation as well as validation against literature can be found in the work by Voet et al. [19]. The certification cumulative effective perceived noise level (EPNL), i.e., the sum of lateral, flyover, and approach EPNL, is used to quantify the noise levels for the derivative and clean-sheet engine designs. The noise levels are estimated on the NASA STCA Standard takeoff and approach trajectory following the work of Berton et al. [11]. Berton et al. denote the Standard trajectory as one that abides by the procedures in ICAO Annex 16 Volume I [20] for subsonic transport-category airplanes. By considering fixed take-off and approach trajectories, any variations in noise levels originate from differences between the derivative and clean-sheet engine designs. Potential noise reductions are possible using variable noise reduction systems [21] such as a programmed thrust cut-back or programed high-lift devices.

III.   Results and Discussion

We first describe the operation of the donor engine core and the associated constraints on the design space of the derivative engine. The impact of these design space constraints on the thrust-specific fuel consumption (SFC), NO_x emissions index [EI(NO_x)], and certification noise levels of the derivative engine relative to a clean-sheet engine are quantified in the subsequent sections.

A.   Donor Engine Core Characteristics

To model the use of the donor engine core in the derivative engine, the operating characteristics of the core need to be determined. The operating conditions of the components on the high-speed core spool from the donor engine are determined by the conservation of mass, power balance between the turbine and compressor on each shaft, and energy balance across the combustor. Using these relations and assuming choked turbines, the core temperature ratio $T_{t4.5}/T_{t2.5}$, the core pressure ratio P_{t45}/P_{t25}, the core inlet corrected mass flow rate $\dot{m}_{2.5}\sqrt{\theta_{2.5}}/\delta_{2.5}$, and the nondimensional fuel flow rate FAR $\times$ LHV$/c_p T_{t2.5}$ can be defined as functions of the corrected high-spool speed $N_H/\sqrt{\theta_{2.5}}$ and the temperature ratio between the high-pressure turbine inlet and the high-pressure compressor inlet $T_{t4.1}/T_{t2.5}$. This relation is given as

$$\frac{T_{t4.5}}{T_{t2.5}}, \frac{P_{t4.5}}{P_{t2.5}}, \frac{\dot{m}_{2.5}\sqrt{\theta_{2.5}}}{\delta_{2.5}}, \frac{\text{FAR} \times \text{LHV}}{c_p T_{t2.5}} = f\left(\frac{T_{t4}}{T_{t2.5}}, \frac{N_H}{\sqrt{\theta_{2.5}}}\right) \quad (2)$$

The thermodynamic stations inside the gas turbine engine are illustrated in Fig. 1. The set of relations in Eq. (2) constitutes the core pumping characteristics. The core temperature ratio and the high spool corrected speed uniquely determine the operating point of the donor core used in the derivative engine. The core pumping characteristics in Eq. (2) can also be recast in terms of other variables such as the temperature ratio $T_{t4.1}/T_{t2.5}$ and the compressor inlet corrected mass flow $\dot{m}_{2.5}\sqrt{\theta_{2.5}}/\delta_{2.5}$. The mass flow rate through the core can be set by any downstream component such as a low-pressure turbine (as in a two-spool engine) or a propulsive nozzle (as in a single-spool turbojet). In the present work, the LPT of the derivative engine determines the mass flow rate through the core and, along with a specified $T_{t4.1}/T_{t2.5}$ ratio, determines the operating point of the core.

B.   Design Space of Derivative Engine

In general, the engine design space is characterized by a set of design parameters: the temperature ratio $T_{t4.1}/T_{t2}$, the fan pressure

ratio π_{fan}, the HPC pressure ratio π_{hpc}, the extraction ratio ER defined as $P_{t1.6}/P_{t6}$, the polytropic efficiency of the various components η_{poly}, and specific attributes for other components such as the mixer, nozzle, and inlet. Thus, the performance metrics such as the specific thrust ($F_n/\dot{m}_a a_0$), SFC, EI(NO_x), and EPNL can be described by the following functional relationship:

$$\frac{F_n}{\dot{m}_a a_0}, \text{SFC}, \text{EI}(NO_x), \text{EPNL}, \ldots$$

$$= f\left(\frac{T_{t4.1}}{T_{t2}}, \pi_{\text{fan}}, \pi_{\text{hpc}}, \text{ER}; \eta_{\text{poly},i}, \eta_{\text{inlet}}, T_{\text{limit}} \ldots\right);$$

$$\text{design variables}: \frac{T_{t4.1}}{T_{t2}}, \pi_{\text{fan}}, \pi_{\text{hpc}}, \text{ER};$$

$$\text{technology specific parameters}: \eta_{\text{poly},i}, \eta_{\text{inlet}}, T_{\text{limit}}, \ldots \quad (3)$$

The turbine inlet to fan inlet temperature ratio ($T_{t4.1}/T_{t2}$), the compressor pressure ratios ($\pi_{\text{fan}}, \pi_{\text{HPC}}$), and extraction ratio are design variables that are chosen to meet specific performance requirements. The polytropic efficiency of the turbomachinery components and the relevant loss metrics for other components such as the inlets, mixers, and nozzles along with material limits (such as temperature limits for compressor and turbine materials) are representative of achievable technology levels. Improvements in these technology parameters will monotonically improve the engine performance in terms of efficiency and fuel consumption, though not necessarily in terms of NO_x emissions.

In the design space of the derivative engine, the HPC pressure ratio is not an independent design variable because the operating point of the high-pressure core in the derivative engine is completely characterized by $T_{t4.1}/T_{t2}$, π_{fan}, and ER, as detailed in Sec. III A. Therefore, for a specified donor core and a set of technology level parameters, the design space of the derivative engine is reduced to the space of possible values for the independent design variables: temperature ratio, fan pressure ratio, and extraction ratio, in other words,

$$\frac{F_n}{\dot{m}_a a_0}, \text{SFC}, \text{EI}(NO_x), \text{EPNL} \ldots = f\left(\frac{T_{t4.1}}{T_{t2}}, \pi_{\text{fan}}, \text{ER}\right) \quad (4)$$

The extraction ratio is kept approximately 1.0 to minimize mixing losses and is usually 1.05–1.07 [22]. For the derivative engine presented in this work, an extraction ratio of 1.06 is chosen, providing the best SFC with the mixer diameter not exceeding the fan diameter. The design space of the derivative engine for typical range of the design variables suitable for a SST aircraft is shown in Fig. 4. The design space shown here represents a slice of the $T_{t4.1}/T_{t2}$ vs π_{fan} plane in the design space at an ER of 1.06.

The region on the right half of the graph, shaded in red, represents the portion of the design space where the nozzle exit flow is supersonic (indicated by the $M = 1.0$ contour) at takeoff condition and would therefore result in increased noise due to shocks in the exhaust flow. The turbine cooling mass flow rates in the core are determined by the donor engine cycle. The fixed cooling flow fractions result in higher blade metal temperatures as the compressor pressure ratio increases, because the cooling bleed air temperature increases. The area of the design space that results in the turbine stator vane and rotor blade metal temperatures exceeding the materials limit ($T_{\text{vane}} > 1278$ K and $T_{\text{blade}} > 1222$ K) is also shaded in red in Fig. 4. Therefore, the feasible design space of the engine is represented by the unshaded region.

Figure 4 shows that the cruise SFC contours for the derivative engine decrease monotonically with decreasing fan pressure ratio, because lower fan pressure ratios lead to lower jet velocities and therefore improved propulsive efficiencies. For a given fan pressure ratio (i.e., fixed x location in Fig. 4; see Appendix C for a graph showing a slice of the design space at $\pi_{\text{fan}} = 2.0$), there is an optimal temperature ratio that minimizes the SFC. However, this point is located in the infeasible region of the design space because the blade temperatures exceed the limits indicated by the shaded regions. The increase in SFC above a certain temperature ratio occurs because
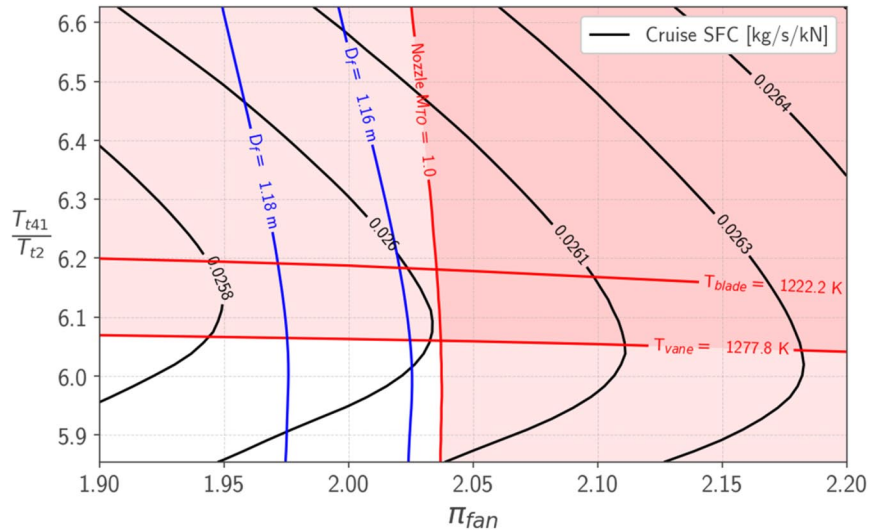
Fig. 4   Design space of derivative engine: $T_{t4.1}/T_{t2}$ vs π_{fan} at the engine aerodynamic design point. The unshaded region represents the feasible design space of the derivative engine. The blue lines show contours of constant fan diameter. The STCA [11] has a fan diameter of 1.16 m (45.5 in.).

increasing the turbine inlet temperature for a fixed thrust requirement forces the high-pressure compressor (from the donor engine) to operate at a lower compressor pressure ratio. This is due to the predefined pumping characteristics of the donor core, as described in more detail in Appendix C.

C.   Design Space of Clean-Sheet Engine

Because the high-pressure spool is purpose designed for the clean-sheet engine, the HPC pressure ratio is an independent design variable, and the high-pressure spool components can be sized separately, allowing for an extra degree of freedom as shown in Fig. 5. We assume that for a purpose-built high-pressure core the components can be designed such that the polytropic efficiencies at the aerodynamic design point are equal to those of the donor engine at its aerodynamic design point (i.e., represent a similar manufacturing and design technology level; this allows us to quantify the performance impact due to the donor core constraints and not the technology level of the components). This means that for every (π_{fan}, $T_{t4.1}/T_{t2}$) combination the HPC pressure ratio is a free variable that can be used to optimize a specific objective, e.g., minimizing cruise SFC (resulting in π_{hpc}^*), or to meet design space constraints, such as the fan size limit or takeoff nozzle exit Mach number. This increased degree of freedom provides better performance relative to the derivative engine. The stator vane and rotor blade temperatures in the high-pressure turbine of the clean-sheet engine are kept below

material limits by sizing the cooling mass flow at the design point. The impact of the ability to size the cooling flow rate to meet the required cooling flow demand at a given temperature ratio and fan pressure ratio is seen in the design space, as the turbine metal temperature limits do not restrict the design space (unlike in the derivative engine). As the fan pressure ratio increases, there is a region of the design space where the nozzle exit Mach number at takeoff is supersonic as demarcated by the white line in Fig. 5.

D.   Engine Performance as Function of Propulsion System Requirements

The previous sections presented the design space of a clean-sheet and derivative engine for a fixed propulsion system thrust requirement set by the STCA airframe. The required thrust (or specific thrust) of the airframe can impact the relative performance of a clean-sheet and derivative engine. The following sections detail the sensitivity of engine performance in terms of SFC, EI(NO$_x$), and EPNL to the design point thrust requirement. The thrust requirement at design is perturbed by $\pm 5\%$ relative to the baseline STCA design point thrust requirement. At each thrust level, the clean-sheet and derivative engines are optimized subject to the constraints shown in Table 2. The constraints applied to all the engines are compressor and turbine metal temperature limits and a nozzle pressure ratio limit to reduce the extent of shock-cell noise at takeoff.

As the specific thrust ($F_N/\dot{m}a_0$) required from the engine is increased, the jet velocity increases, which in turn decreases the
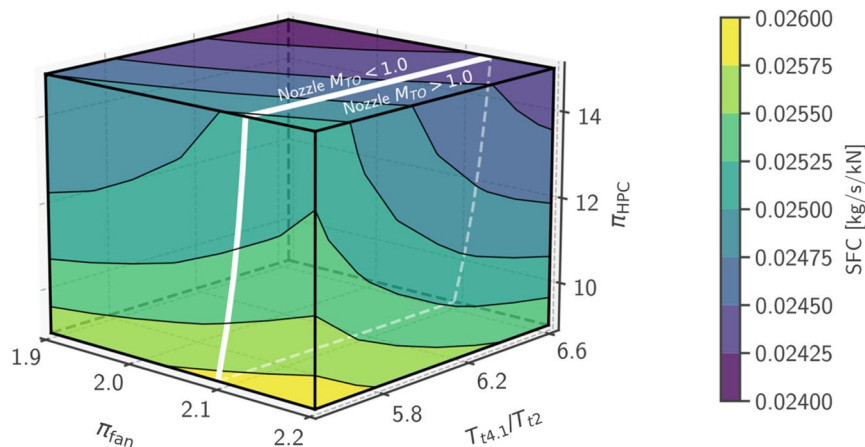

Fig. 5   Design space of clean-sheet engine showing π_{fan}, $T_{t4.1}/T_{t2}$, and π_{HPC} as the three design variables. The minimum SFC occurs at the highest temperature ratio, highest HPC pressure ratio, and the lowest fan pressure ratio. The white lines demarcate the undesirable region of the design space where the nozzle exit Mach number is supersonic at takeoff as annotated in the figure.

Table 2 Optimization objective function and constraints for clean-sheet and derivative engines

Engine	Derivative engine	Clean-sheet engine without NO_x limit	Clean-sheet engine with NO_x limit
Objective function	SFC	SFC	SFC
Constraints	$T_{blade} \leq 1222$ K	$T_{blade} \leq 1222$ K	$T_{blade} \leq 1222$ K
	$T_{vane} \leq 1278$ K	$T_{vane} \leq 1278$ K	$T_{vane} \leq 1278$ K
	$T_{t3} \leq 900$ K	$T_{t3} \leq 900$ K	$T_{t3} \leq 900$ K
	$\left.\frac{P_{r9}}{P_{amb}}\right\|_{takeoff} \leq 2.0$	$\left.\frac{P_{r9}}{P_{amb}}\right\|_{takeoff} \leq 2.0$	$\left.\frac{P_{r9}}{P_{amb}}\right\|_{takeoff} \leq 2.0$
			$EI(NO_x) \leq 14.5$ g/kg

propulsive efficiency and results in an increase in nondimensional corrected fuel flow rate, $f_{corr} = \dot{m}_f \times LHV/(a_0 D^2 p_0)$, as seen in Fig. 6a. Plotting the nondimensional corrected fuel flow rate (as defined by Cumpsty and Heyes [23]) against the specific thrust shows that this trend is independent of fan size (various fan sizes are shown in different colors in Fig. 6a). Figure 6a also illustrates the impact of the takeoff nozzle pressure ratio constraint on the engine cycle; at a specific thrust of approximately 0.164, we observe an increase in the sensitivity

of the corrected fuel flow to the specific thrust. This is because the higher specific thrust requires higher jet velocities while the pressure ratio constraint at takeoff effectively limits the Mach number of the flow at the nozzle exit. Therefore, the temperature of the jet must increase to be able to provide the required jet velocity. This is achieved by a decrease in the work extracted by the LPT and therefore a decrease in the pressure rise of the HPC. This decrease in the cycle pressure ratio further reduces the cycle efficiency (in addition to the decrease in propulsive efficiency due to increased jet velocity). This decrease in HPC pressure rise also results in a sharp decrease in $EI(NO_x)$ in Fig. 6b at a specific thrust of approximately 0.164

Assuming fixed aerodynamic performance (i.e., L/D), the thrust required is directly proportional to the variation in the weight of the aircraft. At a given flight condition, a fixed fan diameter and fan face Mach number set the mass flow rate through the inlet. Therefore, an increase in the thrust required increases the specific thrust that the engine needs to be designed for. The performance of the clean-sheet and derivative engine as a function of the thrust required relative to the baseline STCA for a fixed fan diameter of 1.16 m (45.5 in) based on the STCA airframe [11] is shown in Fig. 7.

The clean-sheet engine designed for minimum SFC subject to material limits results in a 4.9–4.3% improvement in SFC relative to the derivative engine; however, the NO_x emissions index at cruise is
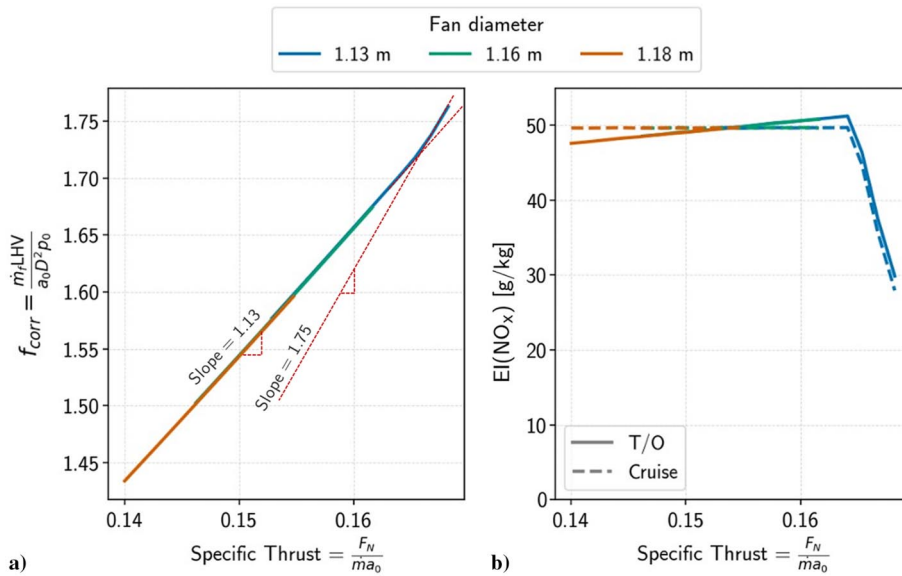

Fig. 6 Nondimensional performance of clean-sheet engine for a range of required specific thrusts and different fan diameters: a) nondimensional fuel flow vs the specific thrust and b) emission index of NO_x vs the specific thrust. The sensitivity of the nondimensional fuel flow to specific thrust is annotated in panel a, highlighting the change in slope when the nozzle Mach number constraint is in effect. The colors represent different engine fan diameters.
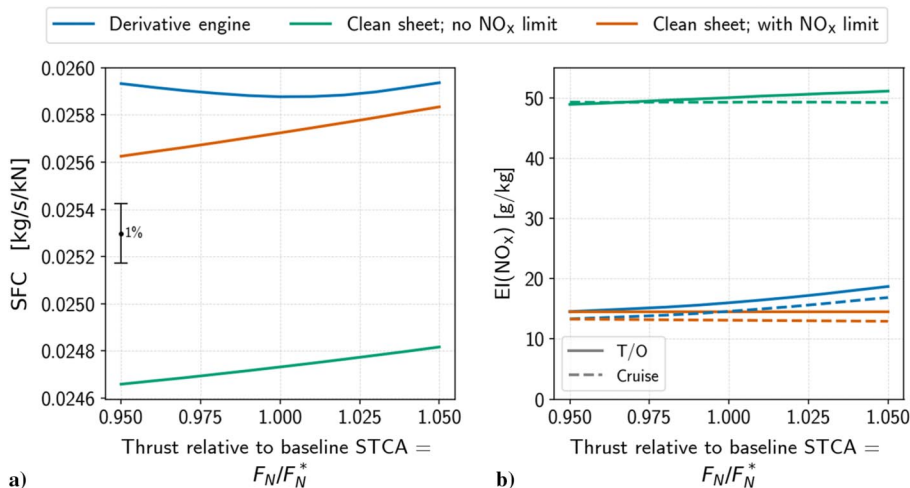

Fig. 7 a) SFC and b) $EI(NO_x)$ of clean-sheet and derivative engines as a function of the thrust required. The thrust required is shown as a fraction of the STCA design thrust.
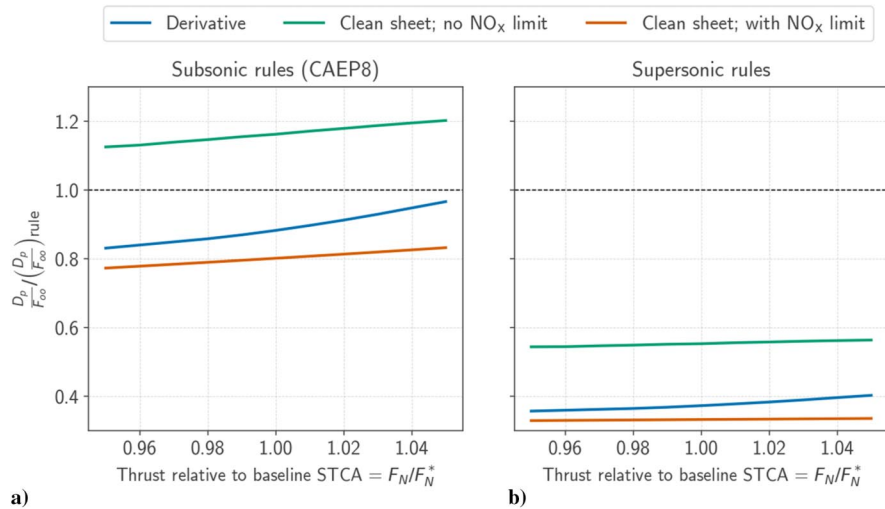
Fig. 8 D_p/F_{oo} relative to the a) subsonic CAEP/8 and b) supersonic rules vs thrust requirement relative to the STCA baseline.

2.2–2.8 times that of the derivative engine. This is because when the clean-sheet design of the engine is only subject to material limits a higher HPC pressure ratio is desirable for increasing the overall cycle pressure ratio and therefore reducing the SFC of the engine. However, the high HPC pressure ratio results in a high temperature and pressure at the inlet of the combustor (P_3, T_3), which results in an increase in the EI(NO$_x$). This represents a tradeoff between the fuel efficiency (and therefore CO_2 emissions) and the emissions of NO$_x$. In the case of the derivative engine, the design space constraints shown in Fig. 4 stemming from turbine material limits (as well as the fixed cooling flow rates from the donor core) limit the HPC pressure ratio such that EI(NO$_x$) for the range of thrusts shown here is 15~20 g/kg.

An alternate clean-sheet design is shown where the engine is optimized for minimum SFC but subject to an EI(NO$_x$) constraint at takeoff of 14.5 g/kg [i.e., the minimum EI(NO$_x$) of the derivative engines for the range of thrusts considered here]. This results in a clean-sheet engine that has a 0.4–1.2% reduction in SFC relative to the derivative engine. The EI(NO$_x$) limit is a more severe constraint on the engine cycle optimization than the last-stage temperature limit of the compressor. This also indicates that improvements in compressor material to withstand higher temperatures are unlikely to result in improvements in performance without resulting in increased NO$_x$ emissions. The resulting LTO emissions metric value (D_p/F_{oo}) based on the current subsonic Committee on Aviation Environmental Protection (CAEP)/8 standards as well as the supersonic standards from ICAO Annex 16 are shown in Fig. 8. A summary of the CAEP/8 limits is provided in Appendix B. The derivative engine presented here would meet the subsonic standard with a 6–18% margin, while the clean-sheet engine simply optimized for minimum SFC would not meet the current subsonic standard. This analysis does not include characteristic correction divisors or other development allowances.

Figure 9 shows the cumulative certification EPNL calculated for each engine using a fixed thrust-setting schedule based on the NASA STCA Standard takeoff and approach trajectories. For engines with higher thrust requirements at design and takeoff, the thrust required at each point of the trajectory is assumed to scale proportionally.

The results show that the EPNL for the derivative and the clean-sheet engines vary by less than 3 EPNdB. The variation in noise levels seen here is driven by the differences in jet velocity at the off-design points between the three engines. The variation in the jet velocity stems from the differences in the thermodynamic cycle of the three different engines considered here. At each design thrust requirement, the derivative and clean-sheet engines have the same specific thrust at the design point because they have the same fan face area, fan face Mach number, and net thrust requirement and therefore the jet velocity at design is identical. However, each engine has a different thermodynamic cycle due to different FPR, HPC pressure ratio, and $T_{t4.1}/T_{t2}$ and consequently have different matching characteristics
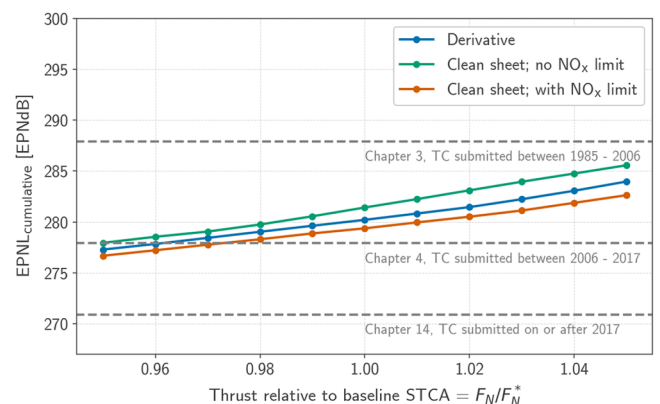

Fig. 9 Standard trajectory EPNL as a function of thrust requirements. Also shown are the chapter 3, 4, and 14 noise levels, shown along with the dates of the type certificate (TC) cutoff when these limits became applicable for new-type aircraft.

Table 3 Summary of derivative and clean-sheet engine design and performance; the clean-sheet engine with NO$_x$ limit is constrained to a takeoff EI(NO$_x$) of 14.5 g/kg; the chapter 4 allowable noise limits are 278 EPNdB

Engine	Derivative engine	Clean-sheet engine without NO$_x$ limit	Clean-sheet engine with NO$_x$ limit
π_f	2.0	2.0	1.95
π_{HPC}	10.0	19.0	9.5
Tt4, K	1828	2000	2000
ER	1.06	1.02	1.03
Cruise SFC, kg/s/kN	0.0259	0.0247	0.0257
Cruise EI(NO$_x$), g/kg	13.0	32.7	9.04
Takeoff EI(NO$_x$), g/kg	16.0	51.6	14.5
Subsonic Dp/Foo, g/kN	35.0	79.2	30.2
CAEP/8 limit, g/kN	39.7	68.1	37.6
Cumulative noise, EPNdB	280.2	281.4	279.4

leading to jet velocity differences of the order of 4–6% during the takeoff trajectory. Because the jet noise is the dominating noise source for high specific thrust engines for SST, small variations in the cumulative EPNL are expected. A summary of the derivative engine and clean-sheet engines is shown in Table 3.

IV. Conclusions

We show that the use of a donor core in the derivative engine imposes constraints on the design space by coupling the operation of

the high-pressure spool with design choices made on the low-pressure spool such as the choice of the fan pressure ratio. Furthermore, we show that the increased degree of freedom obtained in a clean-sheet engine from the high-pressure spool provides design space benefits that can be used to decrease fuel consumption. When only designing for minimum SFC, the clean-sheet engine designed for the STCA thrust requirement results in an SFC improvement of approximately 4.5%. However, such a design has 2.5 times the cruise $EI(NO_x)$ and a 1.2 EPNdB increase in noise relative to the derivative engine. When constraining the clean-sheet engine to have a takeoff $EI(NO_x)$ less than the minimum takeoff $EI(NO_x)$ of the derivative engine (for the range of thrusts considered here), we find that a 0.5% improvement in SFC relative to the derivative is possible with a 0.8 EPNdB decrease in noise and a 10% decrease in cruise $EI(NO_x)$ relative to the derivative engine. With a fixed combustor design, the constraint on the takeoff $EI(NO_x)$ limits the maximum pressure ratio of the thermodynamic cycle, which in turn limits the SFC benefit of using a clean-sheet design. This highlights the need to have advanced low NO_x emissions combustors to be able to reap the SFC benefits of operating at higher overall pressure ratio (OPR) without excessive NO_x emissions.

The more severe limit imposed by the NO_x constraint suggests that improvements in turbine materials, which would reduce the amount of cooling flow required, are more likely to yield performance improvements than improvements in compressor materials. While the current work evaluates the impact of the design space constraints imposed by the donor core on the derivative engine cycle, further reduction in fuel burn is possible with improvements in component efficiencies, and reduction in $EI(NO_x)$ could be possible with the use of advanced combustors. The sensitivity of the performance of a clean-sheet engine relative to a derivative engine to the component efficiencies, material limits, and combustor technology requires further research.

We calculate the Landing and takeoff emissions (LTO) emissions metric value D_p/F_{oo} and compare it against the ICAO Annex 16 Volume II standards for supersonic aircraft (that remain from the Concorde era) to show that these engines can have up to an approximately 65% margin to the standard. This suggests that the NO_x limits for supersonic aircraft are outdated. We also show that the derivative engine and the clean-sheet engine subjected to a NO_x emissions constraint can meet the current CAEP/8 D_p/F_{oo} limits for subsonic aircraft engines. Although we consider a 10% variation in thrust requirement for the clean-sheet and derivative engines, we note that the trends may vary in different ways for larger aircraft cruising at higher Mach numbers, and this should be considered in future research.

Appendix A: Donor Engine Model Details at Sea Level Static

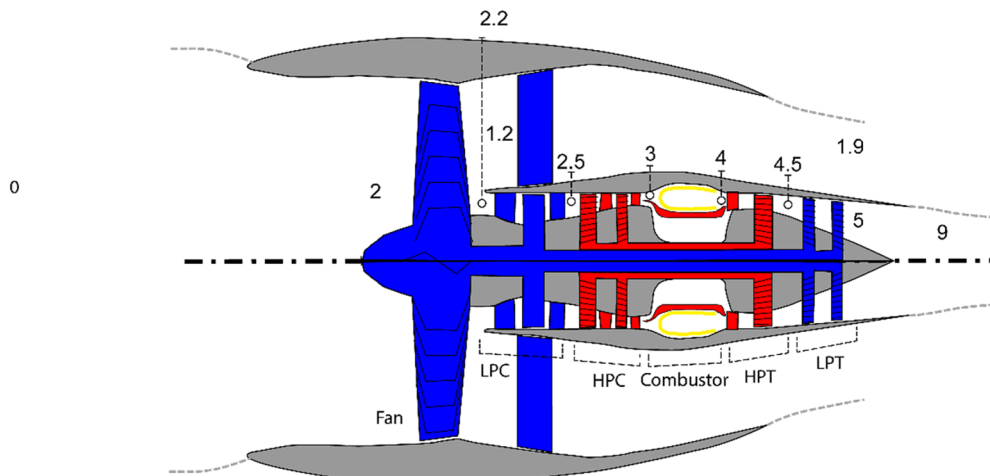**Table A1   Summary of donor engine model at SLS conditions**

Variable	Value
Inlet Mach number	0.0
Altitude, m	0.0
Inlet mass flow rate, kg/s	440
Gross thrust, kN	142.3
Net thrust, kN	142.3
Thrust specific fuel consumption, kg/s/kN	0.0103
Overall pressure ratio	32.6
Combustor exit temperature, T_{t4}, K	1698
Turbine first rotor inlet temperature, $T_{t4.1}$, K	1622

Table A2   Donor engine station data at SLS conditions (refer to Fig. A1 for station numbers)

Station number	Station description	Mass flow rate, kg/s	Corrected mass flow rate, kg/s	Total temperature, K	Total pressure, kPa	Mach number
0	Freestream	440.15	440.15	288.15	101.33	0.00
2	Fan inlet	440.15	441.04	288.15	101.12	0.60
2.2	LPC inlet	68.78	43.78	340.05	172.91	0.40
1.2	Bypass flow	371.38	236.41	340.05	172.91	0.40
2.5	HPC inlet	68.78	25.38	414.78	329.42	0.35
3	HPC exit	63.76	3.31	827.26	3307.35	0.25
3.1	Combustor inlet	53.34	2.77	827.26	3307.35	0.30
4	Combustor exit	54.80	4.24	1697.87	3175.06	0.10
4.5	HPT exit	65.22	16.70	1217.44	813.42	0.35
5	LPT exit	70.24	77.62	842.61	156.79	0.40
9	Core nozzle exit	70.24	78.38	842.61	155.28	0.82
1.9	Bypass nozzle exit	371.38	244.66	340.05	167.09	0.88

Table A3   Donor engine turbomachinery performance at SLS (refer to Fig. A1 for relevant components)

Component	Inlet corrected mass flow rate, kg/s	Pressure ratio	Temperature ratio	Polytropic efficiency	Adiabatic efficiency
Fan	441.04	1.71	1.18	0.93	0.92
LPC	43.78	1.94	1.22	0.95	0.94
HPC	25.38	10.04	1.99	0.91	0.88
HPT	4.24	3.90	1.30	0.87	0.88
LPT	17.12	5.06	1.41	0.87	0.89

Fig. A1   Donor engine schematic showing an unmixed turbofan. Station numbers and key components are highlighted.

Appendix B: ICAO NO$_x$ Emissions Metrics (D_p/F_{oo} [g/kN])

B.1. Supersonic rules

The ICAO supersonic rules limit the NO$_x$ D_p/F_{oo} to be less than

$$\left.\frac{D_p}{F_{oo}}\right|_{\text{limit}} = 36 + 2.42 \times \pi_{oo}$$

B.2. Subsonic CAEP/8 Rules

For engines with $F_{oo} \leq 89$ kN, the ICAO CAEP/8 subsonic rules limit the NO$_x$ D_p/F_{oo} to be below

$$\left.\frac{D_p}{F_{oo}}\right|_{\text{limit}} = \begin{cases} 40.0520 + 1.5681 \times \pi_{oo} - 0.3615 \times F_{oo} - 0.00180 \times \pi_{oo} \times F_{oo}; & \pi_{oo} < 30 \\ 41.9435 + 1.5050 \times \pi_{oo} - 0.5823 \times F_{oo} + 0.005562 \times \pi_{oo} \times F_{oo}; & 30 \leq \pi_{oo} \leq 104.7 \end{cases}$$

Appendix C: SFC Versus Temperature Ratio for Derivative Engines

For the derivative engine, at a given fan pressure ratio, there is a temperature ratio that gives the optimal (minimum) SFC. Figure C1 shows a slice of Fig. 4 at a fan pressure ratio of 2.0.

The nonmonotonic trend in SFC is due to the response of the donor core at different temperature ratios for a fixed thrust requirement. As the temperature ratio increases, the specific power of the donor core also increases. For a fixed thrust requirement and fan pressure ratio (i.e., a fixed location on the x axis in Fig. 4), the mass flow rate through the core must decrease. This mass flow reduction is achieved by decreasing the LPT area, which determines the flow capacity of the LPT and sets the pressure ratio across the HPT (seen from having two turbines in series; see the work by Saravanamuttoo et al. [22]). This reduction in flow capacity and HPT pressure ratio results in the donor core decelerating to a lower corrected speed and compressor pressure ratio. Therefore, as the temperature ratio is increased, there is first an increase in thermal efficiency (from the increase in temperature ratio) but a simultaneous decrease in HPC pressure ratio (which tends to decrease the thermal efficiency), resulting in the observed trend.

Above a temperature ratio of approximately 6.06, the cooling flow rates (determined by the donor core) are insufficient to keep the turbine vanes below the chosen temperature limit. At the selected fan pressure ratio, the minimum SFC occurs in this infeasible region (shaded red in Fig. A4).
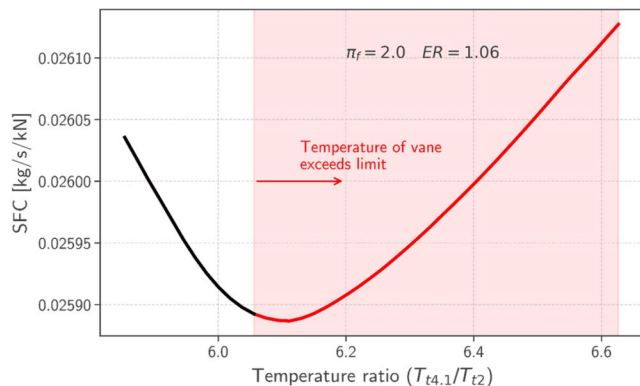

Fig. C1   SFC vs temperature ratio at a fan pressure ratio of 2.0. This figure represents a vertical cut of the design space shown in Fig. 4.

References

[1] Carioscia, S. A., Locke, J. W., Boyd, I. D., Lewis, M. J., and Hallion, R. P., "Commercial Development of Civilian Supersonic Aircraft," 2019, https://www.ida.org/research-and-publications/publications/all/c/co/commercial-development-of-civilian-supersonic-aircraft.

[2] Tang, R., Luther, L., Elias, B., and Morgan, D., "Supersonic Passenger Flights," Rept. R45404, 2018, https://sgp.fas.org/crs/misc/R45404.pdf.

[3] ICAO, *Annex 16 to the Convention on International Civil Aviation: Environmental Protection. Volume II Aircraft Engine Emissions*, International Civil Aviation Organization, https://store.icao.int/en/annexes/annex-16?publication_type=Annex.

[4] Candel, S., "Concorde and the Future of Supersonic Transport," *Journal of Propulsion and Power*, Vol. 20, No. 1, 2004, pp. 59–68. https://doi.org/10.2514/1.9180

[5] Sun, Y., and Smith, H., "Review and Prospect of Supersonic Business Jet Design," *Progress in Aerospace Sciences*, Vol. 90, April 2017, pp. 12–38. https://doi.org/10.1016/j.paerosci.2016.12.003

[6] Eastham, S. D., Fritz, T., Sanz-Morère, I., Prashanth, P., Allroggen, F., Prinn, R. G., Speth, R. L., and Barrett, S. R. H., "Impacts of a Near-Future Supersonic Aircraft Fleet on Atmospheric Composition and Climate," *Environmental Science: Atmospheres*, Vol. 2, No. 3, 2022, pp. 388–403. https://doi.org/10.1039/D1EA00081K

[7] Berton, J. J., Jones, S. M., Seidel, J. A., and Huff, D. L., "Noise Predictions for a Supersonic Business Jet Using Advanced Take-Off Procedures," *Aeronautical Journal*, Vol. 122, No. 1250, 2018, pp. 556–571. https://doi.org/10.1017/aer.2018.6

[8] Jensen, D. T., Brines, G. L., and Blanton, J. C., "Supersonic Transport (SST) Engines," *45th AIAA/ASME/SAE/ASEE Joint Propulsion Conference and Exhibit*, AIAA Paper 2009-4933, 2009. https://doi.org/10.2514/6.2009-4933

[9] Howard, C. E., GE Aviation Debuts Affinity, First Civil Supersonic Engine in 55 Years, https://www.sae.org/news/2018/10/ge-aviation-debuts-affinity-first-civil-supersonic-engine-in-55-years [retrieved 3 Oct. 2022].

[10] Zorumski, W. E., "Aircraft Noise Prediction Program Theoretical Manual," NASA TM-83199 Part 1, 1982.

[11] Berton, J. J., Huff, D. L., Seidel, J. A., and Geiselhart, K. A., "Supersonic Technology Concept Aeroplanes for Environmental Studies," *AIAA Scitech 2020 Forum*, AIAA Paper 2020-0263, 2020. https://doi.org/10.2514/6.2020-0263

[12] Claus, R. W., Evans, A. L., Lylte, J. K., and Nichols, L. D., "Numerical Propulsion System Simulation," *Computing Systems in Engineering*, Vol. 2, No. 4, 1991, pp. 357–364. https://doi.org/10.1016/0956-0521(91)90003-N

[13] ICAO, *ICAO Aircraft Engine Emissions Databank*, Emissions Databank, International Civil Aviation Organization, http://www.easa.europa.eu/

document-library/icao-aircraft-engine-emissions-databank   [accessed June 2022].

[14] Liepmann, H. W., and Roshko, A., *Elements of Gasdynamics*, Wiley, New York, 1957.

[15] Gauntner, J. W., "Algorithm for Calculating Turbine Cooling Flow and the Resulting Decrease in Turbine Efficiency," NASA TM-81453, 1980.

[16] Lieuwen, T., and Yang, V., *Gas Turbine Emissions*, Cambridge Univ. Press, Cambridge, England, U.K., 2013, pp. 1–368.
https://doi.org/10.2514/1.J053061

[17] Norman, P., Lister, D. H., Lecht, M., Madden, P., Park, K., Penanhoat, O., Plaisance, C., and Renger, K., *Development of the Technical Basis for a New Emissions Parameter Covering the Whole Aircraft Operation: NEPAIR*, European Commission, Brussels, 2003, https://cordis.europa.eu/project/id/G4RD-CT-2000-00182.

[18] Fahey, D. W., Keim, E. R., Boering, K. A., Brock, C. A., Wilson, J. C., Jonsson, H. H., Anthony, S., Hanisco, T. F., Wennberg, P. O., Miake-Lye, R. C., Salawitch, R. J., Louisnard, N., Woodbridge, E. L., Gao, R. S., Donnelly, S. G., Wamsley, R. C., Del Negro, L. A., Solomon, S., Daube, B. C., Wofsy, S. C., Webster, C. R., May, R. D., Kelly, K. K., Loewenstein, M., Podolske, J. R., and Chan, K. R., "Emission Measurements of the Concorde Supersonic Aircraft in the Lower Stratosphere," *Science*, Vol. 270, No. 5233, 1995, pp. 70–74.
https://doi.org/10.1126/science.270.5233.70

[19] Voet, L. J. A., Prashanth, P., Speth, R. L., Sabnis, J. S., Tan, C. S., and Barrett, S. R. H., "Sensitivities of Aircraft Acoustic Metrics to Engine Design Variables for Multi-Disciplinary Optimization," *AIAA Journal*, Vol. 60, No. 8, 2022, pp. 4764–4774.
https://doi.org/10.2514/1.J061411%7D

[20] ICAO, *Annex 16—Environmental Protection—Volume I—Aircraft Noise*, International Civil Aviation Organization.

[21] Voet, L. J. A., Speth, R. L., Sabnis, J. S., Tan, C. S., and Barrett, S. R. H., "On the Design of Variable Noise Reduction Systems for Supersonic Transport Take-Off Certification Noise Reduction," *28th AIAA/CEAS Aeroacoustics Conference*, AIAA Paper 2022-3052, 2022.
https://doi.org/10.2514/6.2022-3052

[22] Saravanamuttoo, H. I. H., Rogers, G. F. C., and Cohen, H., *Gas Turbine Theory*, Pearson, Edinburgh, 2017.

[23] Cumpsty, N. A., and Heyes, A., *Jet Propulsion. A Simple Guide to the Aerodynamic and Theormodynamic Design and Performance of Jet Engines*, Cambridge Univ. Press, Cambridge, England, U.K., 2015, pp. 99–113, Chap. 8.

F. Liu
Associate Editor